Proc. of SPIE Vol. 1690, Design of Optical Instruments, ed. D M Aikens, V L Genberg, G C Krumweide, M J Thomas (Sep 1992) Copyright SPIE

A Two-Position IR Zoom Lens with Low F-number and Large Format

James W. Howard
Michael S. Garner
Edward R. Freniere
Ronald D. Stern
Karen L. Armstrong

Telic Optics, Inc.
576 Boston Post Road East
Marlborough, MA

ABSTRACT

We describe the optical, mechanical and servo designs for a motorized, two-FOV (field of view) IR objective lens for use in the 8-12μm spectral band. The FOV is changed by moving lenses axially instead of the more traditional approach which is to add and remove lenses. The advantages of this approach include: simple mechanics, since a single mechanism can be used for both adjusting focus and changing FOV; only one lens group need be moved; no stow space is needed for removed lenses; and fewer total lenses are needed (four elements). The lens is used with a low-cost, uncooled focal plane array. This dictates relatively fast F-number, large image format (F/1.1, 7.8° narrow FOV, 155-mm narrow-field focal length), and low cost. This combination of wide field and large collecting aperture pose a difficult optical design challenge. The lens meets a range of military environmental requirements including immersion in one meter of water. We describe how the requirements were met. We have fabricated and tested five lenses and we describe the assembly and testing process and present a summary of test results.

1. INTRODUCTION

We designed a four-element two-FOV IR lens in which the FOV is changed by moving 3 of the lenses axially as a group. This led to a simple, compact design which featured low weight, low cost and high optical throughput. While it is necessary to move at least two lens groups to achieve a continuous range of focal lengths, two focal lengths can be achieved by moving a single lens group axially. This is a well-known principle and is the basis of stepped power changers in some rifle scopes.[1] The step zoom provides considerable mechanical simplification compared to a continuous zoom and permits a small package size.

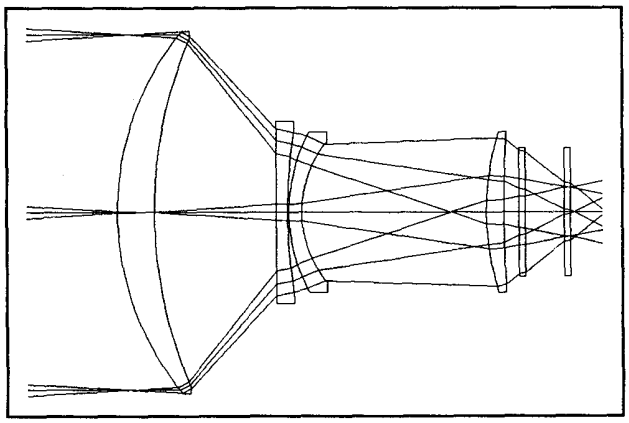

Figure 1 Raytrace showing lens in the narrow field (NFOV) mode.

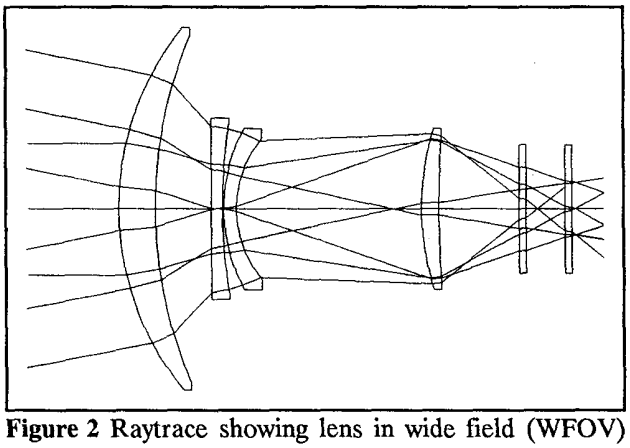

Figure 2 Raytrace showing lens in wide field (WFOV) mode.

2. OPTICAL DESIGN

The optical design is shown in Figures 1 and 2. As indicated in the figures, lens elements 2, 3, and 4 are moved axially about one inch to change FOV. As the lenses are driven from one extreme to the other, the image starts in focus, gradually goes out of focus, then comes back into focus in the other FOV position. By making small changes about the two in-focus positions we can accommodate changes in focus using the same mechanism for both zooming and focusing. Moving the same interior lenses for both FOV change and focus leads to mechanical simplicity because we eliminate a mechanism and avoid the necessity of moving the front lens element or the entire lens for focus. This also makes it easier to seal the lens.

The optical design requirements are different for this lens than for those used in scanning IR systems such as Forward-Looking Infrared (FLIR) systems. There is no scanner and the detector is uncooled so there can be no narcissus. Rays can therefore be allowed to strike lens surfaces at normal incidence. Since there is no cold shield, the system aperture stop need not be placed near the detectors.

The product of the collecting aperture diameter and the field of view is called the Lagrange invariant and is a measure of light gathering power for optical systems. The Lagrange invariant is much larger in this lens than for a typical FLIR. The large collecting aperture is needed to gather more light since uncooled detectors are less sensitive than cooled ones. Table 1 compares the aperture and field of this lens to two Common Module FLIR systems.[2] The large Lagrange invariant makes it difficult to achieve the diffraction-limited performance normally associated with FLIR lenses. This is particularly true with the constraints of low cost and high transmittance. However, the detector instantaneous FOV (IFOV) is large compared to the diffraction-limited resolution so a perfect optical design is not needed. The lens described in this paper has about 1/2 wave of aberration (peak-to-valley) at wavelength 10μm (average over the field).

Table 1 Lagrange invariant compared to Common Module FLIR systems.

System	Diagonal FOV (deg)	Aperture Diameter (mm)	Lagrange Invariant (mm-deg)
AN/TAS-6			
NFOV	2.57	114.3	294
WFOV	7.6	38.1	
TTS			
NFOV	5.6	121.9	683
WFOV	16.9	40.6	
This System			
NFOV	7.8	140.0	1092
WFOV	21.6	52.4	

To determine the tolerances on optical components we did three analyses. First we varied each parameter and observed its effect on the RMS change in wavefront error. This is a traditional way to determine tolerance sensitivities in FLIRs. The problem with this approach is that the RMS wavefront error is not directly related to MTF in systems with 1/2 wave of nominal design wavefront error. We also varied each parameter and observed the effect on MTF directly. This is a good way to determine the effects of individual tolerances on performance, but does not give insight on combining tolerances. We also varied all parameters together and computed the effect on MTF. We found this to be the best way to make performance predictions. We assumed that every tolerance was at either the plus or minus extreme of its allowed range. We perturbed every parameter assigning it at random either a plus or minus error. We then compute the MTF at best focus. This process was repeated one hundred times to determine the average MTF and the standard deviation. Table 2 shows the nominal design and toleranced MTFs.

Table 2 MTF at selected frequencies for the nominal design and after determination of tolerances.

Narrow Field of View				
Spatial Frequency	Nominal Design MTF		Tolerance MTF (mean-σ)	
	On axis	Edge of Field	On Axis	Edge of Field
0.0	1.00	1.00	1.00	1.00
4.0	0.90	0.64	0.87	0.62
8.0	0.79	0.48	0.73	0.44
Wide Field of View				
Spatial Frequency	Nominal Design MTF		Tolerance MTF (mean-σ)	
	On axis	Edge of Field	On Axis	Edge of Field
0.0	1.00	1.00	1.00	1.00
4.0	0.88	0.80	0.82	0.74
8.0	0.64	0.53	0.62	0.51

3. MECHANICAL DESIGN

The lenses are moved by a DC servo motor which drives a precision ball screw via a 9-to-1 gear train. An anti-backlash ball nut is mounted to the screw and the slide tube containing the lenses is fastened to the ball nut with a bracket. A ball screw is used in preference to a lead screw to minimize friction. The 9-to-1 gear ratio was chosen to because it was the highest ratio that would permit the FOV to be changed in about one second. A high gear ratio allows the lenses to be moved slowly for operator-assisted focusing.

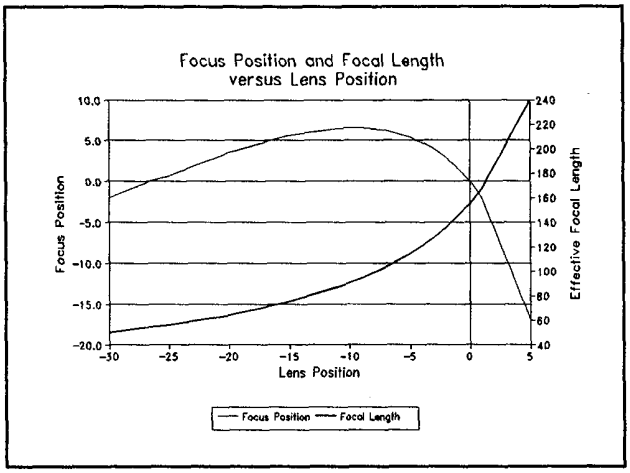

Figure 3 Focus position and focal length versus lens position.

4. THERMAL DESIGN

The lens operates over the temperature range -30° C to +50° C. We used aluminum for all major parts to avoid binding of the mechanisms. We also allowed a diameter clearance of about 10μm between the slide tube and the main bore so thermal gradients could not cause binding. A large focus travel was incorporated to allow thermal defocus to be compensated manually. The resistivity of the germanium in the lens elements was restricted to the range 5-20 ohm-cm to minimize absorption at high temperature.

5. LENS ASSEMBLY

The lenses were assembled by centering them in their mounts with three gauge pins and potting them using RTV. The optical tolerances on centration were of the order ± 0.002". We accurately machined the lens seats and controlled the

lens mounting flats and the centration of the lens mechanical and optical surfaces. This eliminated the need for optical alignment while raising the price of components only slightly.

We selected GE RTV 162 as the potting compound for the lenses. RTV 60 is the more usual choice for potting infrared lenses, but it has the drawback of poor adhesion. A primer is needed to achieve adequate adhesion. RTV 60 is very fluid when it is first mixed so care must be taken to avoid migration of the potting compound. RTV 60 is a two-part mixture and a minute quantity of catalyst is mixed with the RTV silicone to cure. Large quantities of RTV must be mixed to achieve a predictable cure time. RTV 162 does not require a catalyst. It adheres well and can be used without a primer. It is more viscous so it can be dispensed precisely. Its primary drawback is that because it is viscous it tends to collect bubbles and pinholes and so does not make a good seal.

6. LENS SEALING

The lens is sealed air tight. The front and rear lenses are sealed with O-rings under lens retaining rings. A cylindrical cover with O-rings seals the mechanism and circuit boards. We fabricated a hermetic electrical connector by epoxying individual electrical pins into an aluminum plate which we then sealed with an O-ring. Fabricating a connector was faster than ordering a mil-spec connector and provided needed design flexibility.

After building the lens we found two areas where the lens leaked. First, it leaked around the outside of the outer lenses through pinholes in the potting compound and around the threads in the retaining ring. We sealed this leak by wiping potting compound on the threads into which the retaining ring screws. Second, the lens leaked through the pipe thread used to seat the pressure valve. The valve is used to allow the lens to be filled with dry nitrogen. This leak persisted regardless of how tightly the valve was screwed down. We also sealed this leak by wiping potting compound on the threads.

We elected to pressurize the lens to 2 PSI and not to use a pressure relief valve despite the fact that lens would be transported in an unpressurized cargo bay at an altitude of 50,000 ft. We calculated that the outer germanium lens could readily withstand one atmosphere of pressure without damage.

The use of O-ring seals and hard carbon coatings on the exposed lens surfaces allowed the lens to be submerged under water. Pressurizing the lens to 2 PSI was an advantage in testing the lens for leaks. We detected them by wiping soapy water on the seals and inspecting for bubbles. If we had used neutral pressure it would have been necessary to submerge the lens in a water tank, then disassemble it and inspect for water penetration.

7. SLIDE TUBE DESIGN

Three lenses are moved axially to change the FOV and to focus. These lenses are housed in a cylindrical structure that we call a slide tube. The slide tube slides inside a bore in the main housing. There are several issues in the design of a slide tube. One is to achieve a smooth running fit between the slide tube and the bore. The clearance between the slide tube and the bore must be small to avoid decentration of the lenses, but the slide tube must not bind. We hard anodized the main bore, then lapped it to smooth its surface. The slide tube was machined to match the main bore accounting for the thickness of anodize to be applied to the slide tube. A teflon impregnated hard anodize was used for the slide tube. We also applied a thin film of solid lubricant. Both teflon and graphite worked well. The bearing surfaces were limited to small pads on the slide tube. This minimized friction and also provided a pathway for the air to escape that would otherwise be compressed by the slide tube when the FOV was changed.

8. SERVO DESIGN

A position-control loop is used to control the movement of the lenses in changing the FOV. A potentiometer is used as the feedback element.

The lenses must be driven at high speed to change FOV, but at low speed for focus. The DC servo motor must operate over a wide (100-to-1) range of speeds to do both jobs. DC servo motors tend to stall if run at low speed and constant voltage. The back EMF voltage is much smaller than the total voltage in this situation so small variations in the load

cause large speed variations. To avoid this problem we control the velocity of the motor during focusing. This is accomplished by using the same position-control loop that is used for FOV change, but with a timer added. While focusing, the position error signal is increased or decreased (depending on the direction of focus) every few milliseconds so the servo will drive the lenses in the prescribed direction. A stepper motor might be used instead of a DC servo motor because the stepper motor can be driven over a wide speed range without gearing, simplifying the mechanical system. The drawbacks of stepper motors are that they draw a lot of current, make acoustic noise, stall easily, and require more drive electronics than a DC motor. The DC servo motor offers three important advantages: simple electronics, quiet operation, and low current. The servo electronics are contained on three small circuit boards that are mounted inside the lens. The total board area was about 27 square inches. The electronics were packaged very coarsely because we had the space available, because we wanted the flexibility to modify the circuitry, and to keep the temperature of the chips low. Our electronics could have been packaged onto two small boards with a total area of about 18 square inches.

A photograph of a completed lens system is shown in Figure 4.

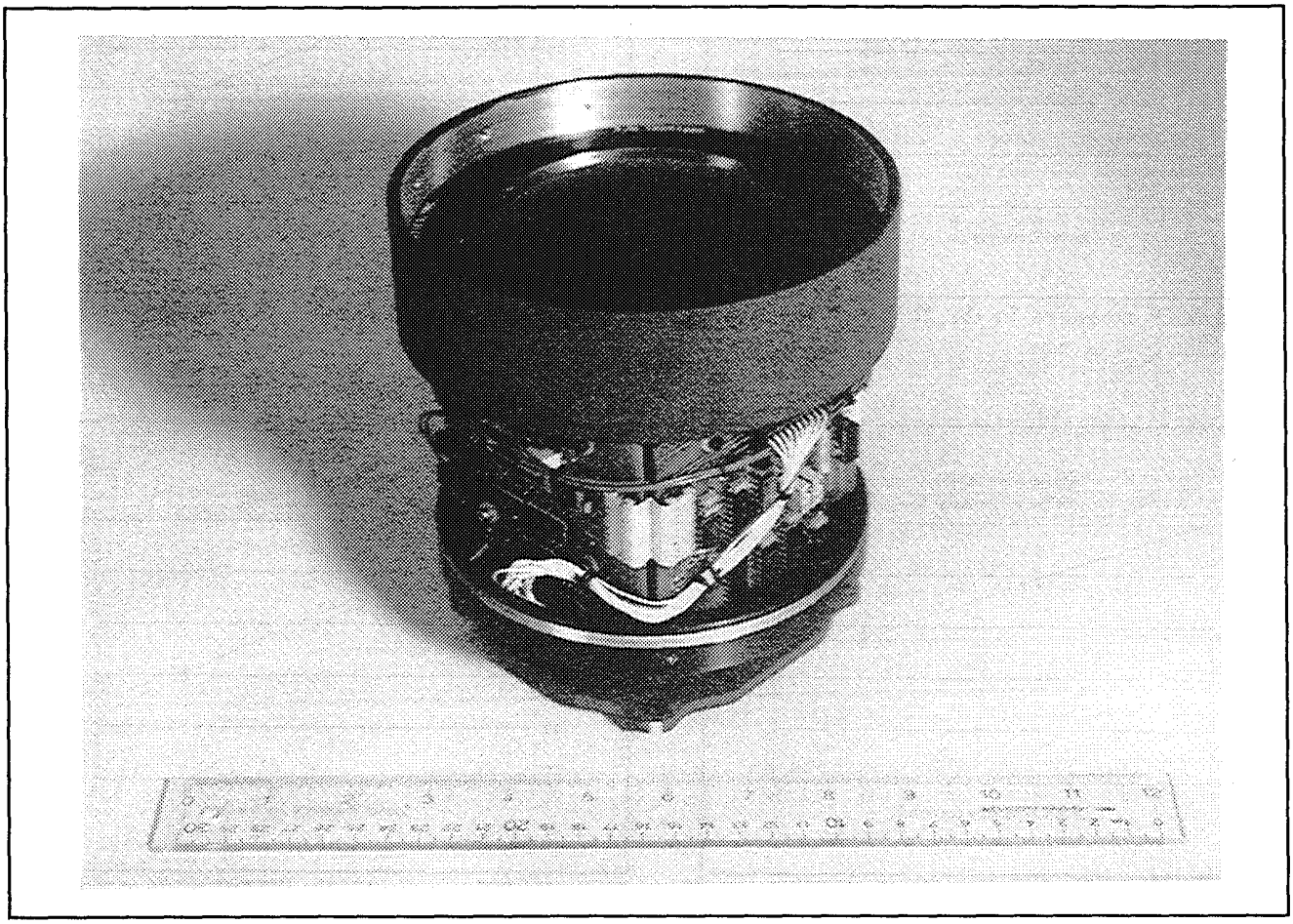

Figure 4 Photograph of a completed lens system.

9. TEST RESULTS

The lens was tested on an automated test station which measured the following lens performance parameters:

- Modulation Transfer Function (MTF)
- F-Number
- System Transmittance

- Distortion
- FOV Change Time

The test station consists of a pinhole source and collimator, a nodal slide lens mount consisting of a rail, rotary table, and a ball slide, a knife edge on a three-axis linear motorized stage, and a detector. By scanning the knife edge across the image and recording the flux passing the knife edge, knife-edge traces are obtained. These traces can be used to compute the line spread function (LSF) and centroid of the image. From the LSF, the MTF and blur size can be calculated, and the centroid location is used in measuring distortion. The tests are described in the following sections.

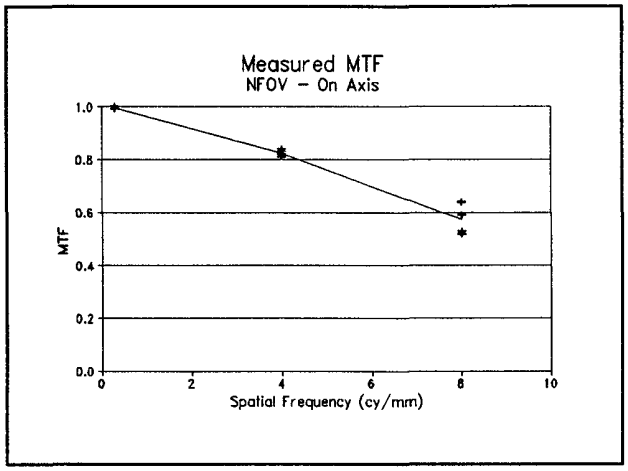

Figure 5 MTF measured in the NFOV mode at the center of the field of view.

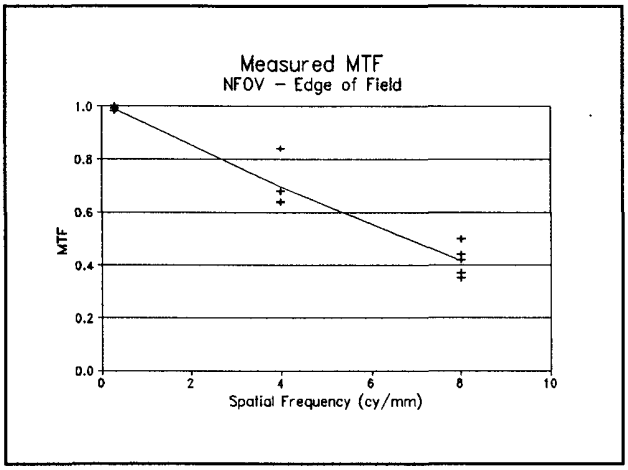

Figure 6 MTF measured in the NFOV mode at the edge of the field of view.

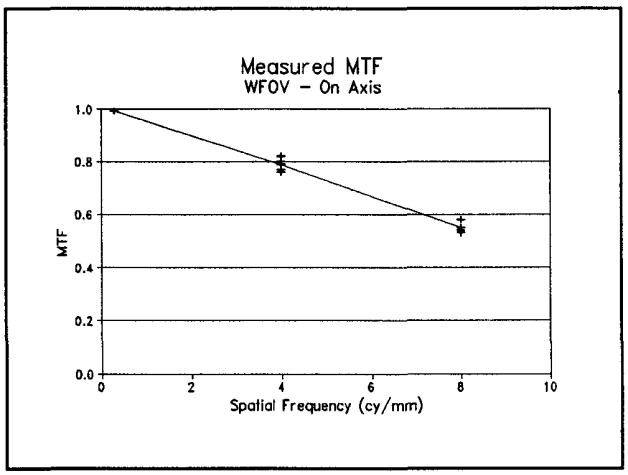

Figure 7 MTF measured in the WFOV mode at the center of the field of view.

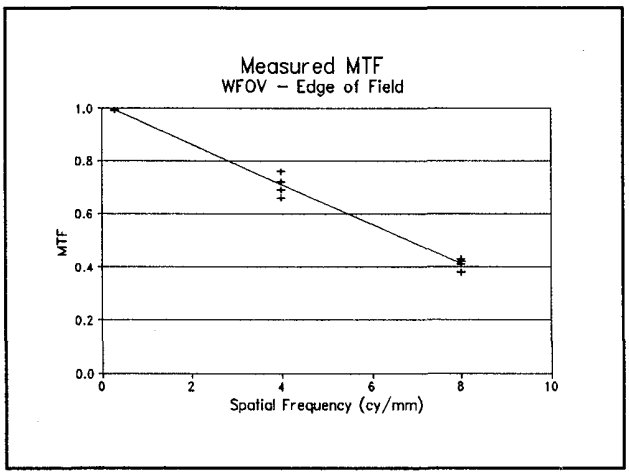

Figure 8 MTF measured in the WFOV mode at the edge of the field of view.

9.1. MTF

The MTF is measured by first obtaining a knife-edge trace of the focused spot, then differentiating the trace to obtain the LSF, and finally Fourier transforming to obtain a cross-section of the MTF. This relation between the LSF and MTF is well known (see, for example, Papoulis[3]).

The MTF was reported at three spatial frequencies. Figures 5-8 show selected values of the measured MTF, namely at the center and edge of the field of view in both the NFOV and WFOV. The line in each figure shows the average value for five units, while the pluses show the actual measured data. Each data point is an average of vertical and horizontal MTF.

9.2. F-Number

The F-number was measured by measuring the throughput of the system with an adjustable iris controlling the diameter of the incident bundle. The throughput was measured as a function of iris diameter, and the diameter at which the throughput began to drop was determined. The EFL was divided by the diameter to determine the F-number.

9.3. System Transmittance

The system transmittance was measured simply by measuring the signal at the detector with and without the system in place, and computing the ratio of these two signals. In order ensure that the incident flux was the same for the two signals, an aperture was placed in front of the system for the system measurement. This aperture has the same area as the integrating sphere used to collect light onto the detector. The F-number and transmittance measurements are summarized in Figure 9.

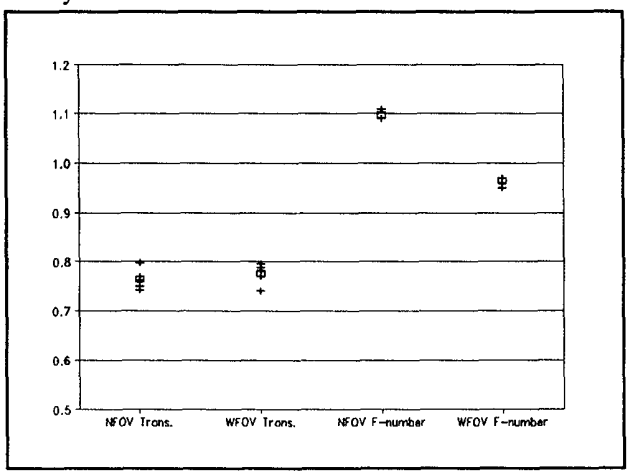

Figure 9 Measured F-number and system transmittance. The pluses are measured data, and the boxes are averages over the five manufactured units.

9.4. Distortion

The distortion was measured at three field points for each field of view. The distortion was measured by rotating the lens off axis about its nodal point as determined from the nominal design focal length. The centroid of the image was determined by knife-edge trace, and the lateral displacement of the image calculated. The linear displacement was divided by the half-field dimension to determine the relative distortion. The data is presented in this way in order that each distortion value is proportional to displacement in the focal plane from the correct image point. The distortion measurements are summarized in Figure 10 for the NFOV and Figure 11 for the WFOV.

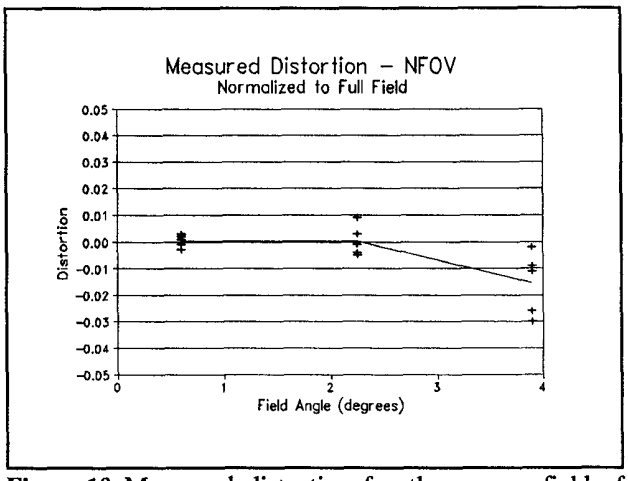

Figure 10 Measured distortion for the narrow field of view mode.

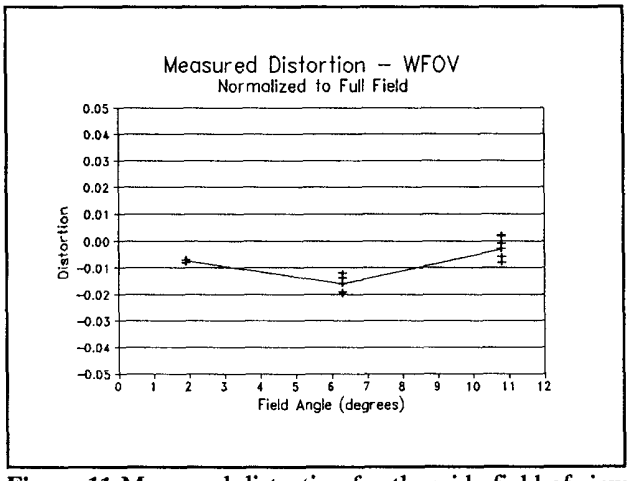

Figure 11 Measured distortion for the wide field of view mode.

9.5. Field of View Change Time

The field of view change time is the time between when the field of view change command is issued and when the lens slide tube reaches the final position. This was measured by connecting a digital storage oscilloscope to the slide tube position feedback voltage, issuing the field of view change command, then measuring the time between the shoulder and the knee of the resulting trace. This test was done for both field of view change commands - changing NFOV to WFOV and WFOV to NFOV. The results are summarized in Figure 12.

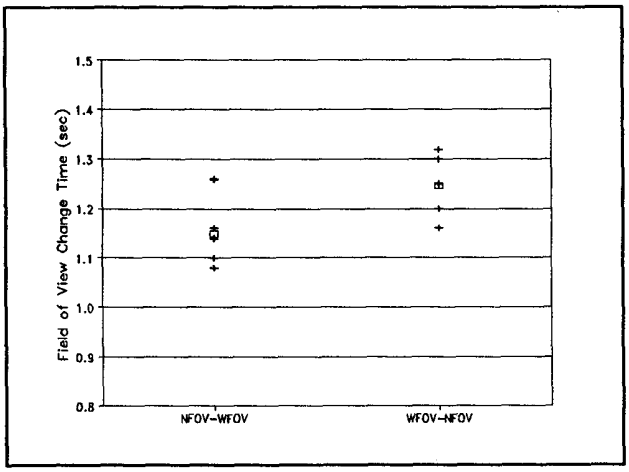

Figure 12 Field of view change time.

10. REFERENCES

1. R. Kingslake, Optical System Design, Academic Press, New York (1978), p. 217.

2. B.D Guenther, R Buser, and W. Morrow, "Electro-Optics in Desert Storm," Optics & Photonics News, (November 1991), p. 8.

3. A. Papoulis, Systems and Transforms with Applications in Optics, McGraw-Hill, New York (1968), pp. 92-93.